

EARLY SIZE DISTRIBUTIONS OF CHONDRULE SUBGROUPS OVERPRINTED BY THE FINAL ACCUMULATION PROCESS OF PARTICLE COMPONENTS IN ALLENDE. K. A. McCain¹, J. I. Simon², J. N. Cuzzi³. ¹The University of Chicago, Chicago, IL 60637, USA (kamccain@uchicago.edu); ²Center for Isotope Cosmochemistry and Geochronology, ARES, EISD-XI3, NASA Johnson Space Center, Houston, TX 77058, USA (justin.i.simon@NASA.gov) ⁴ NASA Ames, Moffett Field, CA 94035, USA (jeffrey.cuzzi@nasa.gov).

Introduction: Populations of compositionally distinct particles are fundamental components of undifferentiated chondritic meteorites [1]. Many theories explain the formation of chondrites, one class of which includes mechanisms for sorting the component particles in the solar nebula prior to their accretion. Mechanisms include sorting by mass [2,3], turbulent concentration [4, Cuzzi et al, this meeting], X-winds [5], and photophoresis [6], which will produce characteristic distributions of observable properties such as particle size. Distinguishing processes that occur in specific astrophysical environments requires characterization of particle types, which include refractory Ca-Al-rich Inclusions (CAIs) and less-refractory chondrules.

Previous investigations of modal abundances of CAIs (e.g., [6,7]) and chondrules (e.g., [3,8]) exist, but differences within and between these two groups, both of which are made up of diverse subgroups with different thermal histories and chemical compositions, remain mostly unstudied. The presence of rims, a significant event occurring after the formation of at least some chondrules, have also yet to be considered with respect to sorting. Here we present the sizes of CAIs and chondrules in Allende with attention to the smallest sizes, subgroups, and particle rims.

Samples and Methods: Components of the Allende CV3 carbonaceous chondrite were characterized using six false-color secondary electron microscope (SEM) X-ray maps obtained by [9,10], with resolutions of 2.88-3.34 $\mu\text{m}/\text{pixel}$ and a total area of 10.08 cm^2 . A sample $\sim 10 \text{ cm}^2$ was also taken from a large $\sim 25 \times 20 \text{ cm}$ slab photographed and characterized by [11], at a resolution of 6.94 $\mu\text{m}/\text{pixel}$. Past work [9-11] attempted to combine data from microscopic scale SEM images with data from a distinct 10 cm^2 region of the large slab [10]. Unfortunately, the smallest particles, particle subclasses, and rims were inconsistently represented or absent. Here we reevaluated the SEM images to include all particles $\geq 25 \mu\text{m}$ and all visible slab particles $\geq 100 \mu\text{m}$. Comparison between larger particle sizes obtained by [10] and equivalent particles in a similarly size slab area allow us to examine slab homogeneity.

Classification. A textural and mineralogical classification scheme was used to define subgroups within the categories of CAI and chondrule and to record rim details in SEM imagery. Particles were grouped into the following categories: a) Porphyritic olivine chondrule (PO), b) Porphyritic olivine and pyroxene chon-

drule (POP), c) Porphyritic pyroxene chondrule (PP), d) Aluminum-rich chondrule, e) Barred olivine chondrule (BO), f) Coarse-grained (CG) chondrule rims, g) fine-grained (FG) chondrule rims, h) Type A CAI, i) Type B CAI, and j) Amoeboid olivine aggregate (AOA). A simpler textural classification scheme was used for the slab data, sorting particles into CAIs, chondrules (with and without rims), and rims (both coarse and fine-grained). These categories correspond to the broadest categories of the SEM classification scheme, so measurements from both can be compared to quantify the distribution of particles over a large range ($\sim 25 \mu\text{m}$ to 1 cm) [12].

Image Processing. Particle size and shape were measured using the ImageJ software. Smaller angular particles that could be particle fragments (e.g., the smallest PO particles) were included in our assessment because their removal has little effect on the curvature of the particle size distributions, as shown by the work of [9]. The diameter of the inner chondrule “core” and the diameter including the rim were measured in rimmed chondrules so that “naked” and “rimmed” chondrules could be compared.

Data compilation. Each data set was normalized to an area of 1,000,000,000 μm^2 to obtain a common scale, and major axis values were binned geometrically. Generally, the SEM data set was most effective at capturing smaller particle sizes and the slab data was more effective at large particle sizes.

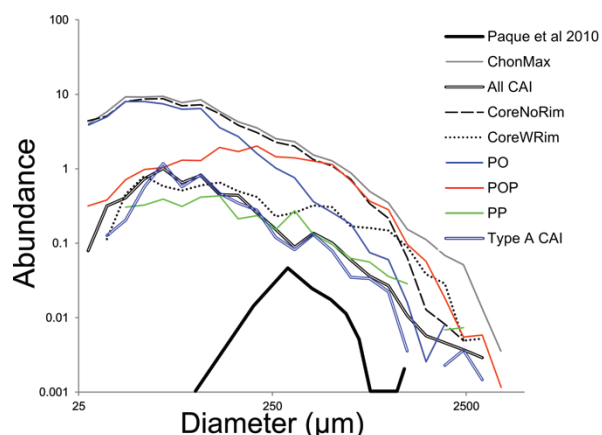


Figure 1. Size distributions of the diameter of chondrules and CAIs in SEM images compared to the narrow range of chondrules reported by those of Paque et al. Particle types defined under *Classification*.

Particle Data Sets. Measurements were made for all of the particle groups described above. Unless stated otherwise each group represents the size of the core without the added thickness of their rims. From this analysis we have chosen to focus on eight data sets for which we could collect enough data to have reasonable confidence. These include: (1) the maximum chondrule size (ChonMax) that includes the rim if present, (2) all CAIs, (3) chondrules (CoreNoRim) with no rims, (4) chondrule cores (CoreWRim) of chondrules with rims, (5) PO cores, (6) POP cores, (7) PP cores, and (8) Type A CAIs.

Unfolding. The integrated 2D data sets were processed using an unfolding algorithm to transform measurements of major axis into particle volumes. This matrix inversion algorithm has been tested by [8] against particle size standard NIST 1019b and against numerically generated 3D particle populations.

Results: Particle Subgroups. Table 1 summarizes the 5193 particles identified in the SEM and slab samples. Area percentages are the sum of CAI, ChonMax, and AOA areas. Particle subgroups vary in average size, though some subgroups (BO and Al-Rich chondrules, Type B CAIs, and AOAs) have too few sampled particles to assume that these averages are representative. Chondrules with rims represented about 31% of all chondrules in the slab. Higher CAI abundance in the slab than SEM data is likely conflation of CAI and AOA particles in the slab data set. The lower chondrule area in the slab likely stems from greater difficulty identifying small particles and fine-grained rims.

Discussion: Broad size distributions. Figure 1 depicts SEM data from chondrules (ChonMax) and CAIs and the most abundant subparticle classes (colored). Slab distributions (not shown) are in general agreement with the SEM data, though phases required for defining subparticle classes could not be identified. In all cases, the size distributions of particles are broad and many particle classes have similar distributions, excepting POP chondrules (abundant at large sizes) and PO chondrules (abundant at small sizes). Type A CAIs are the most common and generally control the CAI distribution, but the largest CAIs are represented primarily by Type B CAIs.

Cores of Rimmed vs Unrimmed Chondrules. In Table 1, chondrule cores with rims (neglecting the thickness of their rims) are on average 64 μm larger than unrimmed cores. This may suggest that rims form preferentially on larger chondrules, but the hypothesis needs further testing. Preliminary analysis also shows that rim thicknesses gradually increase from ~ 0 μm at core sizes < 475 μm to ~ 340 μm at > 1825 μm , shown qualitatively in Figure 1

Data	Particle	Subtype	Count	Avg. Size	Area
SEM	Chondrule			258.4	33.8%
		PO	51.1%	178.4	5.7%
		POP	40.8%	503.4	22.1%
		PP	6.1%	461.7	3.6%
		BO	1.1%	711.8	1.3%
		Al-Rich	0.8%	683.2	1.0%
		Max Size		373.3	46.3%
	CAI			392.8	2.6%
		Type A	86.7%	312	1.4%
		Type B	13.3%	890	1.2%
	AOA			879.1	3.6%
	Total				52.5%
Slab	Chondrule			334.5	26.5%
		W/Rim	30.8%	378.4	11.2%
		No Rim	69.2%	314.8	15.4%
		Max Size		402.4	37.8%
	CAI			404.9	6.6%
	Total				44.4%

Table 1. Modal abundance of particles from SEM and slab data from a sample area approximately 20cm^2

Summary: The similar broad distribution measured between ChonMax, unrimmed core, and CAI distributions suggests that one event or process sorted CAIs, rimless chondrules, and already-rimmed chondrules similarly prior to their incorporation into the chondrite parent body. This event would have overprinted previous differences (e.g., PO vs. POP) that existed between particle types. This also suggests that the rim-forming event for both coarse and fine-grained rims (since both are included in the ChonMax designation) occurred before this final sorting event.

References: [1] Scott et al. (1996) *Chondrules and the protoplanetary disk*, 87-96. [2] Teitler S. A. et al. (2010) *MPS*, 45, 1124-1135. [3] Cuzzi, J. N. et al. (2001) *APJ*, 546, 496-508. [4] Hogan R.C. et al. (1999) *Physical Rev. E*, 60, 1674-1680. [5] Shu F. H. et al. (1996) *Science*, 271, 1545-1552. [6] Wurm G. & Krauss O. (2006), *Icarus*, 180, 487-495. [7] Hezel et al. (2008) *MPS*, 43, 1879-1824. [8] Dodd R.T. (1976) *EPSL*, 30, 281-291. [9] Christoffersen, et al., (2012) *LPSC XLIII*. [10] Fisher, et al., (2014) *LPSC XLV*. [11] Srinivasan et al. (2013) *LPSC XLIV*. [12] Chayes (1954) *Textbook*. [13] Weibel, E. R. (1980) *Stereological Methods; Volume 2: Theoretical Foundations*; Academic Press.